

See discussions, stats, and author profiles for this publication at: <https://www.researchgate.net/publication/224891965>

High-resolution transmission electron microscopy (HRTEM) and X-ray diffraction (XRD) study of the intergrowth in zeolites ITQ-13/ITQ-34

ARTICLE *in* THE JOURNAL OF PHYSICAL CHEMISTRY C · MAY 2009

Impact Factor: 4.77 · DOI: 10.1021/jp900989c

CITATIONS

3

READS

28

6 AUTHORS, INCLUDING:



[Jose L Jorda](#)

Universitat Politècnica de València

65 PUBLICATIONS 1,799 CITATIONS

[SEE PROFILE](#)



[Fernando Rey](#)

Spanish National Research Council

184 PUBLICATIONS 6,576 CITATIONS

[SEE PROFILE](#)



[Khalid Boulahya](#)

Complutense University of Madrid

102 PUBLICATIONS 963 CITATIONS

[SEE PROFILE](#)

High-Resolution Transmission Electron Microscopy (HRTEM) and X-ray Diffraction (XRD) Study of the Intergrowth in Zeolites ITQ-13/ITQ-34

Avelino Corma,*† Maria J. Diaz-Cabanas,† Jose L. Jorda,† Fernando Rey,† Khalid Boulahya,‡ and Jose M. Gonzalez-Calbet‡

Instituto de Tecnología Química (CSIC-UPV), Universidad Politécnica de Valencia, Avenida de los Naranjos s/n, 46022 Valencia, Spain, and Departamento de Química Inorgánica, Facultad de Químicas, Universidad Complutense de Madrid, 28040 Madrid, Spain

Received: February 3, 2009; Revised Manuscript Received: April 2, 2009

Selected area electron diffraction and high-resolution electron microscopy have been used to fully characterize ITQ-13 and ITQ-34. ITQ-13 is made up by a stacking sequence of AAAA... layers along the *a*-axis, while the stacking sequence is ABAB... for ITQ-34. These polytypes can intergrow to crystallize as new materials with different concentrations of each polytype as observed by X-ray powder diffraction. High-resolution images show that in all compositional range both materials intergrow in a disordered sequence along the *a* direction of the ITQ-13.

Introduction

Zeolites are microporous solids that possess a wide range of catalytic industrial uses particularly in oil refining, petrochemicals, and chemicals.¹ Furthermore, zeolites are promising materials in emerging areas, such as nanotechnology.² Their applications are closely related to the structural and compositional characteristics of zeolites; the high microporosity and well-defined pore dimensions allow discrimination between molecules with kinetic diameters differing by less than 0.1 nm. The exact knowledge of the zeolite structure is one of the key parameters in envisaging and understanding the applications of these materials. However, the structure elucidation of zeolites is far from trivial because zeolites usually show very large unit cells presenting low symmetries and containing a large number of atoms. These facts, together with the difficulty in growing zeolites as single crystals in most cases, make their structure resolution a real scientific challenge, especially when only the limited information coming from X-ray powder diffraction (XRPD) data is available for their structure determination. More recently, the combination of XRPD and electron microscopy has represented one step forward for solving complex zeolite structures, as it has been shown in the cases of TNU-9,³ IM5,⁴ and SSZ-74.⁵

Structure resolution can be further complicated because of the tendency of some zeolites to crystallize as intergrowths of different polytypes. The structures of these polytypes share a similar basic layer but present different stacking sequences. This phenomenon has been described for many zeolites, such as zeolite β ,^{6–8} the cubic (FAU) and hexagonal (EMT) polytypes of zeolite Y,^{9–11} the ABC-6 family, which includes 15 different end-members,¹² and the SSZ-33 family,¹³ among others. Additional examples of intergrown zeolites are provided by the International Zeolites Association.¹⁴ The only tools available for studying these intergrowths are model building combined with simulation of XRPD patterns and high-resolution transmission electron microscopy (HRTEM).

In the case of ITQ-13,¹⁵ the structure was determined using single crystal X-ray diffraction data,¹⁶ but structural studies on Ge-containing ITQ-13 were limited to the information obtained from MAS NMR techniques because of the broadening of some particular XRPD peaks, which was attributed to the presence of some structural disorder.¹⁷ Very recently, we have described the structure of a new zeolite, named as ITQ-34,¹⁸ which shows a XRPD pattern very similar to that of the pure ITQ-13. The structure of ITQ-34 presents a basic building layer identical to that in ITQ-13 zeolite but with a different stacking sequence. This opens the possibility of new zeolitic materials based on the intergrowth of these polytypes. Here, we will show that this hypothesis has proven to be correct, since HRTEM shows that blocks of different thickness corresponding to both structural types can intergrow along a common direction.

Experimental Section

ITQ-34 zeolite was prepared according to the procedure previously described.¹⁸ For the ITQ-13 sample and the intergrown materials preparation, the synthesis was performed according to the procedure described in the original paper for ITQ-13,¹⁵ using a synthesis time of 18 days for the intergrown sample containing a ITQ-13/ITQ-34 ratio of 0.3/0.7, named S2, and 40 days for the sample containing a mixture of the intergrowth with a ITQ-13/ITQ-34 ratio of 0.5/0.5, named S3.

X-ray powder diffraction (XRPD) patterns were collected using a Panalytical X'Pert PRO diffractometer in Bragg–Brentano geometry, using Cu K $\alpha_{1,2}$ radiation ($\lambda = 1.5406, 1.5441 \text{ \AA}$) and a X'Celerator detector.

The simulated XRPD patterns of the ITQ-13/ITQ-34 intergrowths were obtained using the program DIFFaX.¹⁹

Selected area electron diffraction (SAED) and high-resolution transmission electron microscopy (HRTEM) were performed using a JEOL 3000 FEG electron microscope fitted with a double tilting goniometer stage ($\pm 22^\circ$, $\pm 22^\circ$). For TEM observations, the crystallites were crushed in an agate mortar, dispersed in acetone, and placed on a holey carbon film. HRTEM observations were performed on a 300 keV electron microscope with Cs = 0.6 mm. Under low beam dose

* To whom correspondence should be addressed. E-mail: acorma@itq.upv.es.

† Universidad Politécnica de Valencia.

‡ Universidad Complutense de Madrid.

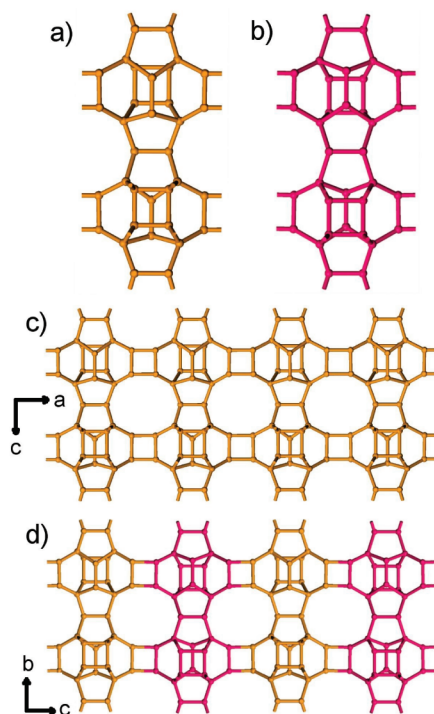


Figure 1. Structure of the sheets in the ITQ-13/ITQ-34 family: (a) basic sheet of ITQ-13 (“sheet A”) viewed along [010]; (b) sheet after the rotation and translation (“sheet B”); (c) stacking sequence AAAA... in ITQ-13; (d) alternate stacking sequence ABAB... in ITQ-34.

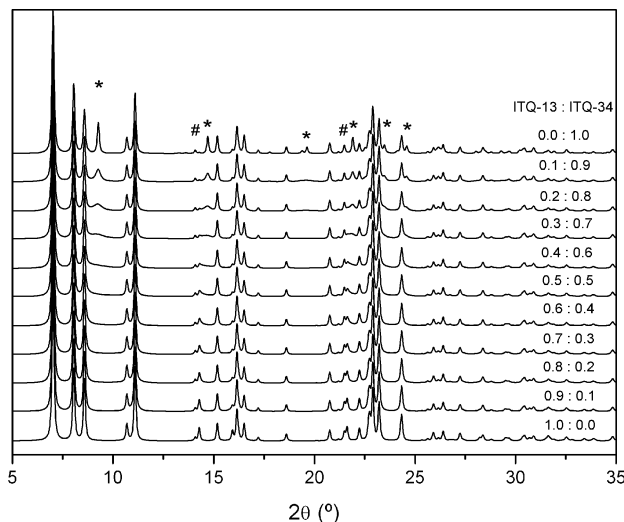


Figure 2. Intergrowths in the ITQ-13/ITQ-34 family simulated with the program DIFFaX: the main differences as highlighted with * for peaks that increase in ITQ-34 and with # for peaks that decrease in ITQ-34.

conditions, the HRTEM images were recorded with a cooled slow-scan Gatan CCD camera.

Results and Discussion

The channel system of the zeolites ITQ-34 and ITQ-13 can be described as a three-dimensional combination of three different channels. The first one is formed by 10-ring straight channels; the second one consists of a circular 10-ring channel system, which intersects the third pore system formed by 9-ring channels.

The structures of ITQ-13 and ITQ-34 polytypes are described in terms of layers in Figure 1. The structure of ITQ-13 consists

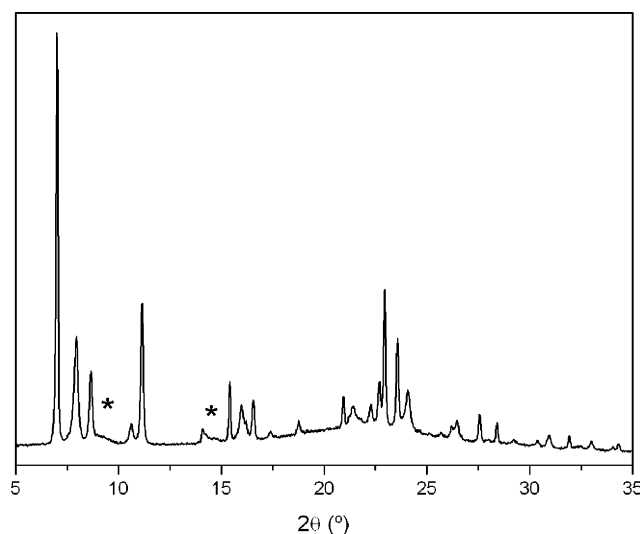


Figure 3. XRPD pattern of a highly intergrown sample of ITQ-13/ITQ-34 (ITQ-13/ITQ-34 ratio close to 0.3/0.7) (sample S2).

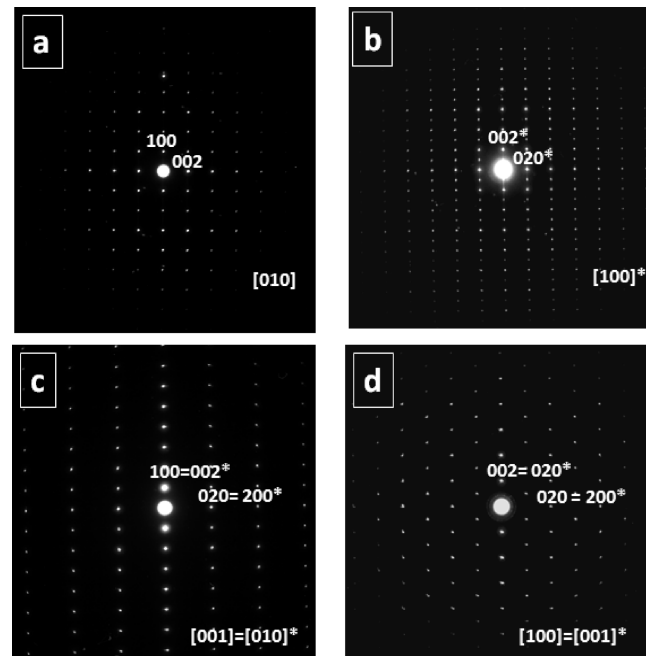


Figure 4. SAED patterns corresponding to ITQ-13 and ITQ-34 along (a) [010] and (b) [100]* zone axes, respectively. (c) [001] = [010]* and (d) [100] = [001]* zone axes are common for both phases. The asterisk (*) refers to the ITQ-34 unit cell.

of repetition of a basic sheet in the *bc* plane (Figure 1a) with a stacking sequence AAAA along the *a*-axis (Figure 1c). In the case of ITQ-34, it is required to define a second basic sheet (Figure 1b), corresponding to the sheet A after a 2-fold rotation around *a*-axis and a subsequent translation of $\frac{1}{2}$ along the *c*-axis; in that case, the stacking sequence is ABAB (Figure 1d).

It is possible to obtain materials with crystals containing intergrowths of both structures because of the existence of a common basis. The XRPD patterns of these “hypothetical” materials have been simulated using the program DIFFaX (Figure 2). One striking characteristic in this family of materials is that even the pure end-member polytypes present extremely similar patterns, with most of the peaks coincident in positions and with similar, although not always equal, relative intensities. Only very subtle differences are observed for the intermediate

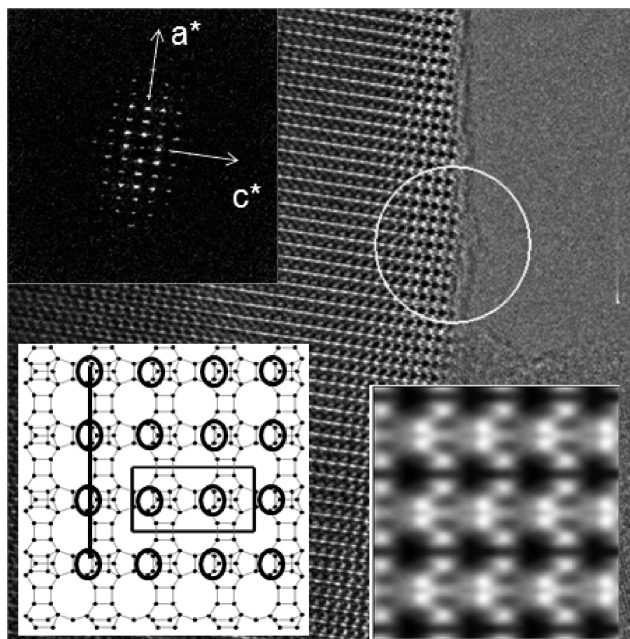


Figure 5. HRTEM micrograph of ITQ-13 along the [010] zone axis. Corresponding FFT and enlarged image of the pore disposition are shown in the inset. Structural model is shown in the inset.

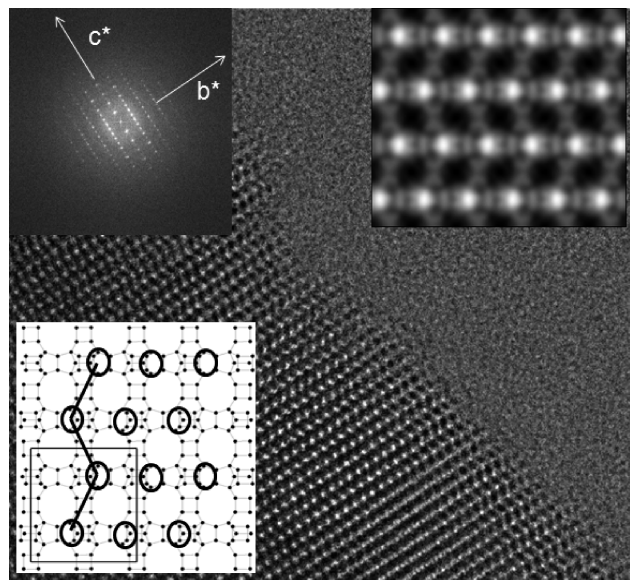


Figure 6. HRTEM micrograph of ITQ-34 along the [100] zone axis. Corresponding FFT and enlarged image of the pore disposition are shown in the inset. Structural model is shown in the inset.

compositions, being extremely difficult to clearly appreciate the presence of new ordered situations even in ITQ-13 samples containing up to 50% of ITQ-34.

In order to further study the possible intergrowth of those structures in a single crystal, a pure ITQ-34 sample, a sample containing pure ITQ-13 crystals, and two intermediate compositions have been selected. In Figure 3, we show the experimental X-ray diffraction pattern obtained for ITQ-13/ITQ-34 in a ratio 0.3/0.7, which is almost identical to the XRPD pattern calculated using DIFFaX simulation program for the same ratio (Figure 2). The peaks marked with an asterisk (*) suggest that both phases are still mixed. In order to know if these phases intergrow inside every crystal, electron microscopy characterization was performed.

Pure ITQ-34 and ITQ-13 samples have been studied by selected area electron diffraction (SAED) to establish the

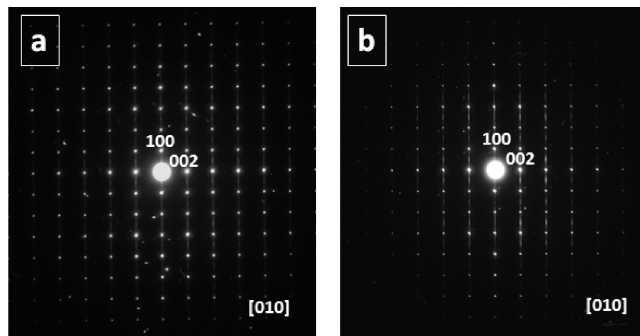


Figure 7. SAED patterns corresponding to samples S2 (a) and S3 (b) along $[010]_{\text{ITQ-13}}$.

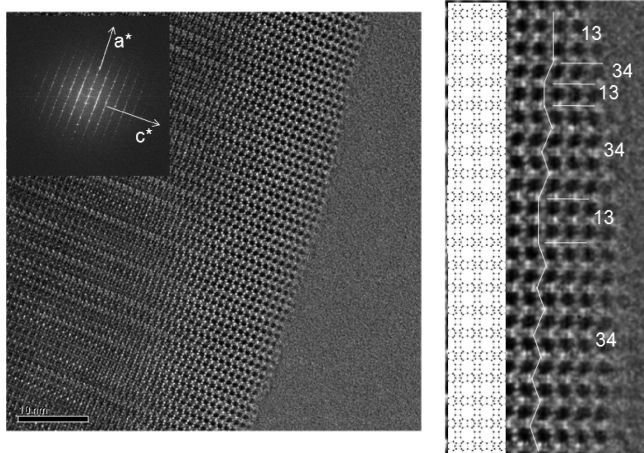


Figure 8. HRTEM micrograph of sample S2 (ITQ-13/ITQ-34 = 0.3/0.7) along the [010] zone axis. Corresponding FFT and enlarged image showing the pore disposition are depicted. Schematic model illustrating the intergrowth is shown in the inset.

crystallographic relation (unit cell parameters and space group) between both materials. From preliminary examination of the SAED pattern of the main zone axis (Figure 4), it was possible to obtain the symmetry and unit cell dimensions of both phases through the analysis of the electron diffraction patterns of several zone axes. Parts a, c, and d of Figure 4 correspond to SAED patterns of ITQ-13 along [010], [001], and [100], respectively, where all maxima can be indexed on the basis of orthorhombic symmetry, with $a = 1.26 \text{ nm}$, $b = 1.16 \text{ nm}$, and $c = 2.19 \text{ nm}$ with space group $\text{Amm}2$ (No. 34), in good agreement with XRPD results described for this material.¹⁶ SAED characterization of ITQ-34 (Figure 4b) shows that this material presents the same basic plane (bc) while the differences remain along the a -axis. This leads to an orthorhombic symmetry, with $a = 1.144 \text{ nm}$, $b = 2.214 \text{ nm}$, and $c = 2.518 \text{ nm}$; the observed systematic absences in the SAED patterns are consistent with a space group Cmcm (No. 63), in good agreement with the structure previously described by XRD for this material.¹⁸ It must be taken into account that in order to use a standard space group, the cell axes in ITQ-13 and ITQ-34 need to be exchanged, with $a_{(\text{ITQ-34})} = b_{(\text{ITQ13})}$, $b_{(\text{ITQ-34})} = c_{(\text{ITQ13})}$, and $c_{(\text{ITQ-34})} = 2a_{(\text{ITQ13})}$.

The HRTEM micrographs corresponding to pure ITQ-13 and ITQ-34 are depicted in Figures 5 and 6 along the [010] and [100] zone axes, respectively. The contrast variation observed shows in both cases an apparently well-ordered material. Fourier transform was performed on the HRTEM images (see insets in Figures 5 and 6) in order to distinguish the existence of different domains that could indicate the presence of different polytypes

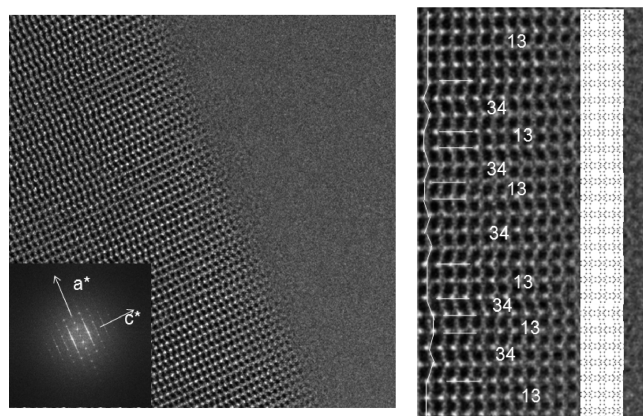


Figure 9. HREM micrograph corresponding to sample S3 (ITQ-13/ITQ-34 = 0.5/0.5) along [010]. Corresponding FFT and enlarged image showing the pore disposition are depicted. Schematic model illustrating the intergrowth is shown in the inset.

or disorder along the structure. However, the whole crystal seems to be homogeneous and only the maxima corresponding to the above-described unit cells are observed. As contrast variation reveals, pore disposition corresponds to the stacking sequence...AAAA... along the *a*-axis for ITQ-13, while a zigzag corresponding to a stacking sequence...ABAB... along the *c*-axis is observed for ITQ-34. In both cases the crystals exhibit platelike shapes, where the growth direction corresponds to the stacking axis. Depicted models for both situations can be seen in the insets of Figures 5 and 6.

The situation is slightly different for the intermediate samples S2 and S3, since strong streaking appears along the *a*-axis (ITQ-13). Actually, SAED patterns are shown in Figure 7 along [010] for S2 (Figure 7a) and S3 (Figure 7b), where strong reflections correspond to the ITQ-13 unit cell. In order to explain such a situation, a HRTEM study was performed on all phases.

The HRTEM results corresponding to samples S2 (ITQ-13/ITQ-34 = 0.3/0.7) and S3 (ITQ-13/ITQ-34 = 0.5/0.5) along the [100] zone axis are depicted in Figures 8 and 9. Fourier transforms performed on the HRTEM micrographs (Figures 8(right) and 9(right)) show a strong streaking along the *a*-axis of ITQ-13, i.e., the *c*-axis of ITQ-34. The contrast variation in both cases can be described as due to strongly disordered materials where blocks of ITQ-13 intergrow with ITQ-34 blocks in a disordered way.

For instance, from contrast variation in sample S2 it can be seen that a large block of ITQ-34 intergrows with blocks of ITQ-13 in a disordered way. However, the situation is slightly different for sample S3, where the concentration of ITQ-13 blocks is similar to that of ITQ-34. An enlarged image corresponding to samples S2 and S3 (insets of Figures 8 and 9) shows the intergrowth between ITQ-13 and ITQ-34, and a schematic model illustrating the intergrowth is shown in the inset.

Conclusions

The ITQ-34 and ITQ-13 zeolites can easily intergrow because of their very similar structures. This resemblance is suggested by the similarity of their XRPD patterns, which explains the problems experienced during the resolution of the pure silica ITQ-13 zeolite using powder diffraction data and in the structural study of Ge-containing ITQ-13.

In this work, we show unambiguously that ITQ-13 and ITQ-34 can be obtained either as pure phases or as intergrown materials.

Electron micrographs suggest that long-range order of both blocks is not obtained, since blocks of different thickness randomly intergrow along the crystals.

Acknowledgment. This work was partially supported by Exxon-Mobil. Financial support from the Spanish Government (Projects MAT2006-14274-C02-01 and MAT2006-08039) and Generalitat Valenciana (Project Prometeo) is gratefully acknowledged. J.L.J. thanks the I3 program of CSIC (Grant 2006801180) for partial financial support.

References and Notes

- (1) Corma, A. *J. Catal.* **2003**, *216* (1–2), 298–312.
- (2) Davis, M. E. *Nature (London)* **2002**, *417*, 813–821.
- (3) Gramm, F.; Baerlocher, Ch.; McCusker, L. B.; Warrender, S. J.; Wright, P. A.; Han, B.; Hong, S. B.; Liu, Z.; Ohsuna, T.; Terasaki, O. *Nature (London)* **2006**, *444*, 79–81.
- (4) Baerlocher, Ch.; Gramm, F.; Massüger, L.; McCusker, L. B.; He, Z.; Hovmöller, S.; Zou, X. *Science* **2007**, *315*, 1113–1116.
- (5) Baerlocher, Ch.; Xie, D.; McCusker, L. B.; Hwang, S.-J.; Chan, I. Y.; Ong, K.; Burton, A. W.; Zones, S. I. *Nat. Mater.* **2008**, *7*, 631–635.
- (6) Newsam, J. M.; Treacy, M. M. J.; Koetsier, W. T.; de Gruyter, C. B. *Proc. R. Soc. London, Ser. A* **1988**, *420*, 375–405.
- (7) Treacy, M. M. J.; Newsam, J. M. *Nature (London)* **1988**, *332*, 249–251.
- (8) Higgins, J. B.; LaPierre, R. B.; Schlenker, J. L.; Rohrman, A. C.; Wood, J. D.; Kerr, G. T.; Rohrbaugh, W. J. *Zeolites* **1988**, *8*, 446–452.
- (9) Breck, D. W. *Zeolite Molecular Sieves*; Krieger: Malabar, FL, 1974.
- (10) Dougnier, F.; Patarin, J.; Guth, J. L.; Anglerot, D. *Zeolites* **1992**, *12*, 160–166.
- (11) Treacy, M. M. J.; Vaughan, D. E. W.; Strohmaier, K. G.; Newsam, J. M. *Proc. R. Soc. London, Ser. A* **1996**, *452*, 813.
- (12) Millward, G. R.; Ramdas, S.; Thomas, J. M. *Proc. R. Soc. London, Ser. A* **1985**, *399* (1816), 57–71.
- (13) Lobo, R. F.; Pan, M.; Chan, I.; Medrud, R. C.; Zones, S. I.; Crozier, P. A.; Davis, M. E. *J. Phys. Chem.* **1994**, *98*, 12040.
- (14) <http://www.iza-structure.org/databases>.
- (15) Boix, T.; Puche, M.; Cambor, M. A.; Corma, A. U.S. Patent 6,471,941 B1, 2002.
- (16) Corma, A.; Puche, M.; Rey, F.; Sankar, G.; Teat, S. J. *Angew. Chem., Int. Ed.* **2003**, *42* (10), 1156–1159.
- (17) Vidal-Moya, J. A.; Blasco, T.; Rey, F.; Corma, A.; Puche, M. *Chem. Mater.* **2003**, *15* (21), 3961–3963.
- (18) Corma, A.; Diaz-Cabanias, M. J.; Jorda, J. L.; Rey, F.; Sastre, G.; Strohmaier, K. G. *J. Am. Chem. Soc.* **2008**, *130*, 16482–16483.
- (19) Treacy, M. M. J.; Deem, M. W.; Newsam, J. M. DIFFaX: A Computer Program for Calculating Diffraction from Faulted Crystals. <http://www.public.asu.edu/~mtreacy/DIFFaX.html>.

JP900989C